Progress In Electromagnetics Research B, Vol. 57, 47–61, 2014

A Mathematical Model for the Transient Lightning Response from Grounding Systems

Zhong-Xin Li*, Yu Yin, Cui-Xia Zhang, and Liu-Cun Zhang

Abstract—With the Fast Fourier Transform (FFT), a mathematical model for accurately computing distribution of a lightning currents flowing along a high voltage a.c. substation's grounding system buried in half infinite homogenous earth has been developed in this paper. It is a hybrid of Galerkin's method of moment (MoM) and a conventional nodal analysis method. The model can directly calculate the distribution of both branch and leakage currents along the grounding system. A dynamic state complex image method and a closed form of Green's function of a dipole or monopole in the half infinite homogenous earth model are introduced into this model to accelerate calculations of mutual impedance and induction coefficients. Analytical formulae for the mutual induction and impedance coefficients have been developed to accelerate the calculation for near field case by using Maclaurin expansion. With the inverse FFT, the model can be used to study the transient lightning response of a grounding system.

1. INTRODUCTION

For lightning protection system earth termination, grounding systems are often used, whose basic function is to disperse the lightning current to earth without causing any potential differences or induced voltages that might endanger people or damage installations. The behavior of grounding systems at power frequencies is well understood and detailed procedures for their design are widely accepted [1]. However, the performance of grounding systems due to lightning strokes might be quite different, and in some cases it the efficiency of the protection can critically deteriorate. In spite of the large amount of work that has been devoted to this subject, there is still no consensus on how to apply our current knowledge to the design of the grounding for better high frequency and dynamic performance [2].

Recently many computerized analysis methods have been developed based on different approaches to research the response of grounding systems to lightning strokes, for example, circuit theory method [3–6], transmission line theory method [7–13], electromagnetic field theory method [14–22], hybrid method [23–26], and finite difference time domain method (FDTD) [27, 28]. Among these numerical methods, the last hybrid method has combined the merits of circuit theory and electromagnetic field theory methods, and can directly calculate the distribution of both branch and leakage currents, better than both circuit theory and electromagnetic field theory methods, further calculating field domain is much less than the one for the FDTD, so it will be deeply studied in this paper.

The hybrid method has been adapted from quasi-static electromagnetic field theory to high frequency electromagnetic field theory. The hybrid method based on quasi-static electromagnetic field theory has been widely used to study substation grounding problem in the low frequency domain in [29–32]. Meanwhile, the hybrid method has further been used to study the lightning problem for grounding system in [23–25]. On the other hand, the hybrid method based on high frequency electromagnetic field theory has been developed to research the lightning problems on a substation's grounding electrodes in [26]. However, that paper gives no details about how to achieve the combination of contributions

Received 19 October 2013, Accepted 18 November 2013, Scheduled 21 November 2013
* Corresponding author: Zhong-Xin Li (zxli@fudan.edu.cn).
The authors are with the China Electric Power Research Institute, No. 15, East Road, Xiaoying, Qinghe, Haidian, Beijing, China.

from the transversal current and longitudinal current, and does not give the Green's function for a dipole buried in homogenous earth model. In this paper, the hybrid method has been systematically described to study the behavior of high frequency electromagnetic fields of the grounding problem with more details about the hybrid method and the Green's function of the dipole buried in the homogenous earth model. On the other hand, the hybrid method is similar to the partial element equivalent (PEEC) method which was developed a long time ago [33, 34].

The complex image method has been well developed in the microwave domain [35–39]. It has been introduced into the electrical power system domain since 1992 by Chow et al. [40]. Due to different electromagnetic field theories applied to grounding system, the complex image method can be divided into three categories: 1) electrostatic complex image method (ESCIM) [40, 41]; 2) quasi-static complex image (QSCIM) [30–32, 42, 43]; and 3) dynamic state complex image method (DSCIM). For the ESCIM in [40, 41], the electrostatic complex image appeared with some pairs of conjugate complex numbers or real numbers, and for the QSCIM in [30–32, 42, 43], the quasi-static complex image used pairs of conjugate complex numbers or complex numbers. We should point out that no matter whether ESCIM or QSCIM is used, the multilayered earth model must be considered as more than two layers of the horizontal conductive medium. However, for DSCIM, all multilayered earth models must be considered, including a homogenous earth model. It can be proved that no pairs of conjugate complex numbers appear for DSCIM. Furthermore, for DSCIM, a shift complex image method has been introduced to deal with Sommerfeld's integral in [44]. However, how to achieve exponential series about an equivalent coefficient of propagation haven't been introduced. The complex image method has been mentioned to study the lightning problem for a grounding electrode without a detailed discussion in [26]. Next, details for both vertical and horizontal dipoles and scalar monopoles in the homogenous earth model will be discussed in this paper.

In this paper, following the above works, based on the high frequency dynamic state electromagnetic field theory and unequal-potential mathematical supposition, and combined with the FFT, a novel accurate model which is a hybrid of the conventional nodal analysis and Galerkin's MoM has been developed for calculating the distribution of both branch and leakage currents along a grounding system in the half infinite homogenous earth model, within which the interaction mutual induction between leakage currents and branch currents has been considered. On the other hand, both branch and leakage currents within the grounding system and their mutual coupling influence are considered in the model. Due to the high frequency electromagnetic field, there is a Sommerfeld infinite integration in vector Green's function of a dipole or scalar Green's function of a monopole. To accelerate the calculation, the high frequency DSCIM and a closed form of these Green's function are introduced, meanwhile, some analytical formulae will be developed to quickly calculate the mutual inductive and conductive coefficients for near field. In this way, the efficiency of our method has been achieved. Meanwhile, with the inverse FFT, the model can calculate the distribution of a lightning current along a grounding system, which can be used to study the transient lightning response of a grounding system.

2. FREQUENCY DOMAIN ANALYSIS

The transient problem is first solved by a formulation in the frequency domain. The time-domain response is then obtained by application of a suitable Fourier inversion technique. The response to a steady state, time harmonic excitation is computed for a wide range of frequencies starting at zero Hz. From this frequency response, a transfer function is constructed for every frequency considered. The transfer function is dependent only on the geometric and electromagnetic properties of the grounding system and its environment.

If $i(t)$ represents the injected current at a point in the grounding system, and $x(t)$ denotes the observed response, then

$$x(t) = F^{-1}W(j\omega) \cdot F[i(t)] \tag{1}$$

where F and F^{-1} are the Fourier and inverse Fourier transforms, respectively, $W(j\omega)$ is the transfer function, and ω is the angular frequency.

Once the transfer functions $W(j\omega)$ have been determined for each calculated quantity, for example the electric field or current at specified points, the time-domain solutions can be obtained by direct

application of Eq. (1). The calculation of the inverse Fourier transform is carried out by an FFT algorithm which is well-suited for the evaluation of the time-domain responses.

The impulse impedance, an essential parameter in grounding system design, is used, which has defined in [45].

3. MATHEMATICAL MODEL OF THE EQUIVALENT CIRCUIT OF THE GROUNDING SYSTEM

The grounding network's conductors are assumed to be completely buried in half homogenous earth with conductivity σ_1 and permittivity $\varepsilon_1 = \varepsilon_r \cdot \varepsilon_0$.

The methodology proposed is based on the study of all the inductive, capacitive and conductive couplings between the different grounding system conductors. First, the grounding system is divided into N_l segments that can be studied as elemental units, then the discrete grounding system has N_p nodes.

The grounding network is energized by injection of single frequency currents at one or more nodes. In general, we consider that a sinusoidal current source of value $\overline{F_m}$ is connected at mth ($m = 1, 2, \ldots, N_p$) node, where scalar electric potential (SEP) $\overline{V_m}$ of the mth node of the grounding network refers to the infinite remote earth as defining zero SEP. In the same way, we define an average SEP $\overline{U_n}$ on nth ($n = 1, 2, \ldots, N_l$) segment. If the segments are short enough, it is possible to consider $\overline{U_n}$ as approximately equal to the average of the nth segment's two terminal nodes SEP: $\overline{U_n} = (\overline{V_l} + \overline{V_m})/2$, where l and m are the nodes of the nth segment.

3.1. Mathematical Model of the Grounding System in Frequency Domain

With the above considerations, and following [25–32], the obtained electric circuit may be studied using the conventional nodal analysis method [46], resulting in the following equations:

$$\left[\bar{\mathbf{F}}\right] = \left[\bar{\bar{\mathbf{Y}}}\right] \cdot \left[\overline{\mathbf{V_n}}\right] \tag{2}$$

$$\left[\bar{\bar{\mathbf{Y}}}\right] = \left[\bar{\bar{\mathbf{K}}}\right]^t \cdot \left[\overline{\overline{\mathbf{Y_s}}}\right] \cdot \left[\bar{\bar{\mathbf{K}}}\right] + \left[\bar{\bar{\mathbf{A}}}\right] \cdot \left[\overline{\overline{\mathbf{Y_b}}}\right] \cdot \left[\bar{\bar{\mathbf{A}}}\right]^t \tag{3}$$

where $[\bar{\mathbf{F}}]$ is an $N_p \times 1$ vector of external current sources; $[\overline{\overline{\mathbf{Y}_b}}]$ is the $N_l \times N_l$ branch admittance matrix of the circuit including resistive and inductive effects, which gives a matrix relationship between branch currents $[\overline{\mathbf{I_b}}]$; $[\overline{\overline{\mathbf{Y_s}}}]$ is an $N_l \times N_l$ mutual conduction matrix, which gives a matrix relationship between average SEP $[\bar{\mathbf{U}}]$ and leakage currents $[\overline{\mathbf{I_s}}]$ through the rapid Galerkin's MoM [41]. The distribution between branch and leakage currents can be seen in Fig. 1. Both $[\bar{\bar{\mathbf{A}}}]$ and $[\bar{\bar{\mathbf{K}}}]$ are incidence matrices, which are used to relate the branches and nodes. They are rectangular matrices of order $N_l \times N_p$, for whose elements, can be referred to [25–32].

The vector of nodal SEP $[\overline{\mathbf{V_n}}]$ may be calculated through solving (2). Refer to [25, 30] and for the method of obtaining the average SEP $[\bar{\mathbf{U}}]$, leakage current $[\overline{\mathbf{I_s}}]$, branch voltage $[\overline{\mathbf{U_b}}]$, and branch current $[\overline{\mathbf{I_b}}]$.

Once the branch and leakage currents are known, the SEP, electrical field intensity (EFI), and magnetic field intensity (MFI) at any point in the half homogenous earth can be calculated.

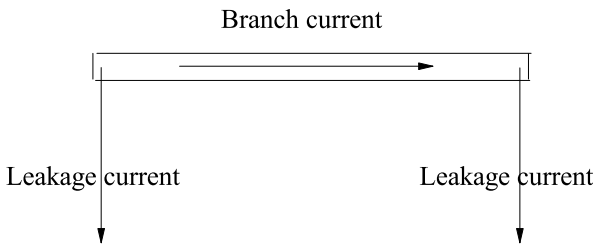

Figure 1. The branch and leakage currents.

Just as in [30–32], the study of the grounding system's performance has been reduced to the computation of $[\overline{\overline{\mathbf{Y_s}}}]$ and $[\overline{\overline{\mathbf{Y_b}}}]$.

3.2. Computation of $[\overline{\overline{\mathbf{Y_b}}}]$ and $[\overline{\overline{\mathbf{Y_s}}}]$

From [25–32], we know that each segment is modeled as a lumped resistance and self-inductance. Mutual inductances or impedances between branch or leakage currents are also included in the model:

$$\left[\overline{\overline{\mathbf{X_q}}}\right]_{N_l\times N_l} = \begin{bmatrix} X_{1,1} & \dots & X_{1,i} & \dots & X_{1,j} & \dots & X_{1,N_l} \\ \vdots & \vdots & \vdots & \vdots & \vdots & \vdots & \vdots \\ X_{i,1} & \dots & X_{i,i} & \dots & X_{i,j} & \dots & X_{i,N_l} \\ \vdots & \dots & \vdots & \dots & \vdots & \vdots & \vdots \\ X_{j,1} & \dots & X_{j,i} & \dots & X_{j,j} & \dots & X_{j,N_l} \\ \vdots & \dots & \vdots & \dots & \vdots & \vdots & \vdots \\ X_{N_l,1} & \dots & X_{N_l,i} & \dots & X_{N_l,j} & \dots & X_{N_l,N_l} \end{bmatrix}^{-1} \tag{4}$$

(i) for $[\overline{\overline{\mathbf{X_q}}}] = [\overline{\overline{\mathbf{Y_b}}}]$ case: $X_{m,m} = Z^s_{mm} + j\omega L_{mm}$, $X_{n,m} = j\omega M_{nm}$; here $m = 1, \dots, N_l$, $n = 1, \dots, N_l$.

The diagonal elements consist of self impedance and self induction, other elements belong to mutual induction between a pairs of conductor segments. The formula for self impedance and self induction can be referred to [25–32], here, we give out formula of mutual induction as below

$$\begin{aligned} M_{nm} &= \int_{l_n}\int_{l_m} \hat{t}_n(\bar{r}_n)\cdot\bar{\bar{G}}_A(\bar{r}_n,\bar{r}_m)\cdot\hat{t}_m(\bar{r}_m)dt_m dt_n \\ &= \int_{l_n}\int_{l_m} \hat{t}_n(\bar{r}_n)\cdot\begin{bmatrix} G^x_{A_{x11}}(\bar{r}_n,\bar{r}_m) & 0 & 0 \\ 0 & G^y_{A_{y11}}(\bar{r}_n,\bar{r}_m) & 0 \\ G^z_{A_{x11}}(\bar{r}_n,\bar{r}_m) & G^z_{A_{y11}}(\bar{r}_n,\bar{r}_m) & G^z_{A_{z11}}(\bar{r}_n,\bar{r}_m) \end{bmatrix}\hat{t}_m(\bar{r}_m)dt_m dt_n \end{aligned} \tag{5}$$

where $\hat{t}_m(\bar{r}_m)$ and $\hat{t}_n(\bar{r}_n)$ are unit direction vectors along the mth and nth short thin conductors, respectively. And $\bar{r}_m$ and $\bar{r}_n$ are position vectors at the surface of mth and nth short thin conductors, respectively.

If a vector dipole buried in an infinite homogenous conductivity medium, the $\bar{\bar{G}}_A(\bar{r}_n,\bar{r}_m) = \frac{\mu}{4\pi}\frac{e^{-jkR_{nm}}}{R_{nm}}\bar{\bar{I}}^0$, here $\bar{\bar{I}}^0$ is a diagonal unit matrix, and $R_{nm} = \sqrt{(x_n-x_m)^2+(y_n-y_m)^2+(z_n-z_m)^2}$, we have

$$M_{nm} = \frac{\mu}{4\pi}\int_{l_n}\int_{l_m}\frac{e^{-jkR_{nm}}}{R_{nm}}\hat{t}_n(\bar{r}_n)\cdot\hat{t}_m(\bar{r}_m)dt_m dt_n \tag{6}$$

For the quasi-static state electrical field case, the electromagnetic wave's propagation effect can be neglected, we know

$$M_{nm} = \frac{\mu}{4\pi}\int_{l_n}\int_{l_m}\frac{1}{R_{nm}}\hat{t}_n(\bar{r}_n)\cdot\hat{t}_m(\bar{r}_m)dt_m dt_n \tag{7}$$

From [31], we know the mutual induction coefficient (7) can be analytically calculated [47, 48]; however, the mutual impedance coefficient (6) can also be analytically calculated, which will be introduced later.

(ii) for $[\overline{\overline{\mathbf{X_q}}}] = [\overline{\overline{\mathbf{Y_s}}}]$ case: $X_{n,m} = Z_{nm}$.

Z_{nm} is the mutual impedance coefficient between a pair of segments in the grounding system. The matrix above includes the conductive and capacitive effects of the earth, and its elements are the mutual impedance coefficient Z_{mn}.

$$Z_{nm} = \int_{l_n}\int_{l_m} G_\varphi(\bar{r}_n,\bar{r}_m)\frac{dt_m}{l_m}\frac{dt_n}{l_n} \tag{8}$$

For an infinite homogeneous conductivity medium, we have $G_\varphi(\bar{r}_n, \bar{r}_m) = \frac{e^{-jkR_{nm}}}{4\pi\bar{\sigma}_1}\frac{1}{R}$ and $\bar{\sigma}_1 = \sigma_1 + j\omega\varepsilon_1$, so

$$Z_{nm} = \frac{1}{4\pi\bar{\sigma}_1 l_m l_n}\int_{l_n}\int_{l_m}\frac{e^{-jkR_{nm}}}{R_{nm}}dt_m dt_n \tag{9}$$

For the quasi-static state electrical field case, since the electromagnetic wave's propagation effect has been neglected, we know

$$Z_{nm} = \frac{1}{4\pi\bar{\sigma}_1 l_m l_n}\int_{l_n}\int_{l_m}\frac{1}{R_{nm}}dt_m dt_n \tag{10}$$

From [31], we know the mutual impedance coefficient (10) can be analytically calculated [47, 48]; however, the mutual impedance coefficient (9) can also be analytically calculated, which will be introduced later.

4. THE CLOSED FORM OF THE GREEN'S FUNCTION OF A SCALAR MONOPOLE OR VECTOR DIPOLE IN THE HALF HOMOGENOUS EARTH MODEL AND THE DYNAMIC STATE COMPLEX IMAGE METHOD

From [49, 50], we have the vector and scalar Green's function of a vertical dipole and a monopole:

$$G^z_{A_{z11}}(\rho, z; \rho', z') = \frac{\mu}{4\pi}\int_0^\infty \frac{k_\rho}{jk_{z_1}}\left[e^{-jk_{z_1}|z-z'|} - k_{01}^{TM}e^{-jk_{z_1}(z'+z)}\right]J_0(k_\rho\rho)dk_\rho \tag{11}$$

where $\rho = \sqrt{x^2+y^2}$, $\rho' = \sqrt{x'^2+y'^2}$; and (x, y, z) and (x', y', z') are, respectively, numerical value of coordination for source and field points. Meanwhile, $k_{01}^{TM} = \frac{\bar{\sigma}_1 k_{z_0} - \bar{\sigma}_0 k_{z_1}}{\bar{\sigma}_1 k_{z_0} + \bar{\sigma}_0 k_{z_1}}$.

$$G_{\varphi_{11}}(\rho, z; \rho', z') = \frac{1}{4\pi\bar{\sigma}_1}\int_0^\infty \frac{k_\rho}{jk_{z_1}}\left[e^{-jk_{z_1}|z-z'|} - k_{01}^{\varphi}e^{-jk_{z_1}(z+z')}\right]J_0(k_\rho\rho)dk_\rho \tag{12}$$

where $k_{01}^{\varphi} = \frac{\bar{\sigma}_0 k_{z_0} - \bar{\sigma}_1 k_{z_1}}{\bar{\sigma}_0 k_{z_0} + \bar{\sigma}_1 k_{z_1}}$.

Meanwhile, the vector Green's function of a horizontal dipole along the x-axis is

$$G^x_{A_{x11}}(\rho, z; \rho', z') = \frac{\mu}{4\pi}\int_0^\infty \frac{k_\rho}{jk_{z_1}}\left[e^{-jk_{z_1}|z-z'|} - k_{01}^{TE}e^{-jk_{z_1}(z'+z)}\right]J_0(k_\rho\rho)dk_\rho \tag{13}$$

where $k_{01}^{TE} = \frac{k_{z_0} - k_{z_1}}{k_{z_0} + k_{z_1}}$.

$$G^z_{A_{x11}}(\rho, z; \rho', z') = \frac{\mu}{4\pi}\frac{\partial}{\partial x}\int_0^\infty \left[-\frac{k_{01}^{TM} + k_{01}^{TE}}{k_\rho}e^{-jk_{z_1}(z+z')}\right]J_0(k_\rho\rho)dk_\rho \tag{14}$$

or

$$G^z_{A_{x11}}(\rho, z; \rho', z') = \frac{\mu}{4\pi}\frac{\partial}{\partial x}\int_0^\infty \frac{k_\rho}{jk_{z_1}}\left[-jk_{z_1}\frac{k_{01}^{TM} + k_{01}^{TE}}{k_\rho^2}e^{-jk_{z_1}(z+z')}\right]J_0(k_\rho\rho)dk_\rho \tag{15}$$

First, the closed form of Green's function of a vertical dipole in Eq. (11) is considered. Using [35–36] and applying the Matrix Pencil (MP) method [51], we develop k_{01}^{TM} into a finite exponential series:

$$k_{01}^{TM} = \tilde{k}_{01}^{TM} + \sum_{i=1}^{M^{TM}}\alpha_i^{TM}e^{\beta_i^{TM}jk_{z_1}} \tag{16}$$

where $\tilde{k}_{01}^{TM} = \frac{\bar{\sigma}_1 - \bar{\sigma}_0}{\bar{\sigma}_1 + \bar{\sigma}_0}$, which is the quasi-static term of k_{01}^{TM}.

$$\begin{aligned} G^z_{A_{z11}}(\rho, z; \rho', z') = \frac{\mu}{4\pi}\int_0^\infty \Bigg[&\frac{k_\rho}{jk_{z_1}}e^{-jk_{z_1}|z-z'|} - \tilde{k}_{01}^{TM}e^{-jk_{z_1}(z'+z)} \\ &- \sum_{i=1}^{M^{TM}}\alpha_i^{TM}\frac{k_\rho}{jk_{z_1}}e^{-jk_{z_1}(z'-\beta_i^{TM}+z)}\Bigg]J_0(k_\rho\rho)dk_\rho \end{aligned} \tag{17}$$

Considering the Sommerfeld identity,

$$\int_0^\infty \frac{k_\rho}{jk_{z_1}} e^{-jk_z|z|} J_0(k_\rho\rho) dk_\rho = \frac{e^{-jkR_0}}{R_0} \tag{18}$$

and Lipschitz integration

$$\int_0^\infty e^{-zk_\rho} J_0(k_\rho\rho) dk_\rho = \frac{1}{R_0} \tag{19}$$

where $R_0 = \sqrt{\rho^2 + z^2}$, we have

$$G^z_{A_{z11}}\left(\bar{r}, \bar{r'}\right) = \frac{\mu}{4\pi}\left[\frac{e^{-jk_1R}}{R} - \frac{\tilde{k}^{TM}_{01}}{R'} - \sum_{i=1}^{M^{TM}} \alpha_i^{TM} \frac{e^{-jk_1R_i^{TM}}}{R_i^{TM}}\right] \tag{20}$$

where

$$R = \sqrt{(x-x')^2+(y-y')^2+(z-z')^2}, \quad R' = \sqrt{\begin{array}{l}(x-x')^2+(y-y')^2\\ +(z+z')^2\end{array}},$$
$$R_i^{TM} = \sqrt{(x-x')^2 + (y-y')^2 + (z-\beta_i^{TM} + z')^2}.$$

We must point out that the complex image method and the closed form of Green's function have been much used in the microwave domain [35–39]. Here, the complex image method has further been introduced into the electrical power system domain to analyze the behavior of a high frequency electromagnetic field, meanwhile, according to the characteristics of the complex image method applied in the electrical power system domain, the complex image method has been called DSCIM.

Then, the closed form of Greens function of a monopole and a horizontal dipole in Eqs. (12), (13) and (14) are considered. Just as for k_{01}^{TM}, all these k_{01}^{φ}, k_{01}^{TE}, and $jk_{z_1}\frac{k_{01}^{TM}+k_{01}^{TE}}{k_\rho^2}$, can be developed into finite terms of exponential series, and applying Sommerfeld identity, Lipschitz integration and its varied form $\int_0^\infty e^{-zk_\rho} J_0(k_\rho\rho)\frac{dk_\rho}{k_\rho} = \ln(z + \sqrt{z^2+\rho^2})$, we have

$$G_{\varphi_{11}}\left(\bar{r}, \bar{r'}\right) = \frac{1}{4\pi\bar{\sigma}_1}\left[\frac{e^{-jk_1R}}{R} - \frac{\tilde{k}^{\varphi}_{01}}{R'} - \sum_{i=1}^{M^{\varphi}} \alpha_i^{\varphi} \frac{e^{-jk_1R_i^{\varphi}}}{R_i^{\varphi}}\right] \tag{21}$$

where $R_i^{\varphi} = \sqrt{(x-x')^2 + (y-y')^2 + (z-\beta_i^{\varphi} + z')^2}$.

$$G^x_{A_{x11}}\left(\bar{r}, \bar{r'}\right) = \frac{\mu}{4\pi}\left[\frac{e^{-jk_1R}}{R} - \sum_{i=1}^{M^{TE}} \alpha_i^{TE} \frac{e^{-jk_1R_i^{TE}}}{R_i^{TE}}\right] \tag{22}$$

where $R_i^{TE} = \sqrt{(x-x')^2 + (y-y')^2 + (z-\beta_i^{TE} + z')^2}$.

$$G^z_{A_{x11}}\left(\bar{r}, \bar{r'}\right) = \frac{\mu}{4\pi}\frac{\partial}{\partial x}\left[-\tilde{k}^{TM}_{01}\ln\left(\left(z+z'\right)+R'\right) - \sum_{i=1}^{M^{TEM}} \alpha_i^{TEM} \frac{e^{-jk_1R_i^{TEM}}}{R_i^{TEM}}\right] \tag{23}$$

where $R_i^{TEM} = \sqrt{(x-x')^2 + (y-y')^2 + (z-\beta_i^{TEM} + z')^2}$.

For the quasi-static electrical field case, since the electromagnetic wave's propagation effect can be neglected, we have

$$G^z_{A_{z11}}\left(\bar{r}, \bar{r'}\right) = \frac{\mu}{4\pi}\left[\frac{1}{R} - \frac{\tilde{k}^{TM}_{01}}{R'}\right] \tag{24}$$

$$G^x_{A_{x11}}\left(\bar{r}, \bar{r'}\right) = \frac{\mu}{4\pi}\frac{1}{R} \tag{25}$$

$$G^z_{A_{x11}}\left(\bar{r},\bar{r'}\right) = \frac{\mu}{4\pi}\frac{\partial}{\partial x}\left[-\tilde{k}^{TM}_{01}\ln\left(\left(z+z'\right)+R'\right)\right] \tag{26}$$

$$G_{\varphi_{11}}\left(\bar{r},\bar{r'}\right) = \frac{1}{4\pi\bar{\sigma}_1}\left[\frac{1}{R}-\frac{\tilde{k}^{\varphi}_{01}}{R'}\right] \tag{27}$$

The vector and scalar Green's functions $G_{A_{z11}}(\bar{r},\bar{r'})$, $G_{A_{x11}}(\bar{r},\bar{r'})$, $G^z_{A_{x11}}(\bar{r},\bar{r'})$, and $G_{\varphi_{11}}(\bar{r},\bar{r'})$ for the quasi-static electrical field case can be found in [31].

5. HOW TO QUICKLY CALCULATE ANALYTICALLY THE ELEMENTS OF $[\overline{\overline{Y}}_b]$ AND $[\overline{\overline{Y}}_s]$ FOR THE HIGH FREQUENCY ELECTROMAGNETIC FIELD CASE

The M_{mn} in Eq. (6) and Z_{mn} in Eq. (9) are, respectively, the mutual induction and impedance coefficients. In the general case, we introduce the symbol A_{mn} to denote M_{nm} and Z_{mn}, so we have

$$A_{mn} = \int_{l_m}\int_{l_n}\frac{e^{-jkR_{nm}}}{R_{nm}}dt_m dt_n, \tag{28}$$

Here $m=1, \ldots, N_l$, $n=1, \ldots, N_l$, and $R=\sqrt{\begin{matrix}(x_n-x_m)^2+(y_n-y_m)^2\\+(z_n-z_m)^2\end{matrix}}$.

For two short conductors l_m and l_n at any position, we can write their line parameter equations as follows: l_m: $x = x_m(t_m) = a^x_m t_m + b^x_m$, $y = y_m(t) = a^y_m t_m + b^y_m$, $z = z_m(t_m) = a^z_m t_m + b^z_m$; and l_n: $x = x_n(t_n) = a^x_n t_n + b^x_n$, $y = y_n(t_n) = a^y_n t_n + b^y_n$, and $z = z_n(t_n) = a^z_n t_n + b^z_n$.

Thus, we have

$$A_{mn} = \int_{l_m}\int_{l_n}\frac{e^{-jk\sqrt{t_m^2+2\beta t_m+\gamma}}}{\sqrt{t_m^2+2\beta t_m+\gamma}}dt_m dt_n \tag{29}$$

where $\beta = -(a^x_m a^x_n + a^y_m a^y_n + a^z_m a^z_n)t_n + (a^x_m b^x_m + a^y_m b^y_m + a^z_m b^z_m) - (a^x_m b^x_n + a^y_m b^y_n + a^z_m b^z_n) = -\xi t_n + \zeta$; and $\gamma = t_n^2 + 2[(a^x_n b^x_n + a^y_n b^y_n + a^z_n b^z_n) - (b^x_m a^x_n + b^y_m a^y_n + b^z_m a^z_n)]t_n - 2(b^x_m b^x_n + b^y_m b^y_n + b^z_m b^z_n) + (b^x_m)^2 + (b^y_m)^2 + (b^z_m)^2 + (b^x_n)^2 + (b^y_n)^2 + (b^z_n)^2 = t_n^2 + 2\psi t_n + \chi$.

Here, we can use the Maclaurin series to expand the X_{nm}, so an analytical formula can be obtained instead of the numerical integration, this will be introduced below.

According to the Maclaurin series, we have

$$\begin{aligned}A_{mn} = \int_{l_m}\int_{l_n}\Bigg[&\frac{1}{\sqrt{(t_m+\beta)^2+\gamma-\beta^2}} - jk - \frac{k^2\sqrt{(t_m+\beta)^2+\gamma-\beta^2}}{2} + \frac{jk^3\left((t_m+\beta)^2+\gamma-\beta^2\right)}{6} + \ldots\\ &+\frac{(-jk)^{\eta}\sqrt{((t_m+\beta)^2+\gamma-\beta^2)^{\eta-1}}}{\eta!} + \ldots + \frac{(-jk)^{N_t}\sqrt{\left((t_m+\beta)^2+\gamma-\beta^2\right)^{N_t-1}}}{N_t!}\Bigg]dt_m dt_n,\end{aligned} \tag{30}$$

Here, $\eta = 0, 1, 2, \ldots, N_t$, and N_t is the maximum number of the Maclaurin series, which is chosen by the desired precision of the calculation. We must point out that the first term can analytically calculated [47, 48, 52], however, others must be carefully studied. After some examination, we can see that the above formula consists of two kinds of pieces of basic integral formulae:

$$T_1(\eta) = \int_{l_1}^{l_2} t^{\eta}\ln\left(f+bt+\sqrt{t^2+Q^2}\right)dt, \tag{31}$$

$$T_2(\eta) = \int_{l_1}^{l_2} t^{\eta}\sqrt{t^2+Q^2}dt, \tag{32}$$

Both of the two formulae can be solved analytically, which have been fully discussed in [53].

6. NUMERICAL RESULTS AND ANALYSIS

According to the approach introduced in this paper, a Fortran language program has been implemented, which can simulate any complicated grounding system in a half infinite homogenous earth model.

6.1. Verification of Model

To verify the results of the method proposed in this work, some cases solved by other authors [55–58] are studied. Although our mathematical model was designed to calculate the behavior of high frequency electromagnetic fields within a grounding system, the model can also calculate the behavior of a low frequency electromagnetic field in the grounding system. To verify our model, numerical results for both high and low frequency electromagnetic fields will be observed through different comparisons.

6.1.1. Low Frequency Domain Case

The first case is from [55], in which the unequal potential model is used. The earth is homogenous, whose conductivity is 100^{-1} S/m, the size of the grounding grid is 60 m × 40 m and consists of a 6×4 mesh grid, the material of the conductor is Cu, whose conductivity is $5.8 \times 10^{+7}$ S/m, and whose radius is 10 mm, and is buried at a depth of 0.5 m. The potential at injecting point is 960.9 V from [55], the calculated maximum value of SEP at injecting point are, respectively, (963.2, 2.720) V for the quasi-static electrical field case and (951.9, −7.569) V for the dynamic state electromagnetic field case, and the minimum values of SEP at the grid are, respectively, (962.4, −1.016) V for the quasi-static electrical field case and (951.1, −11.235) V for the dynamic state electromagnetic field case. In the calculation, the permittivity of the earth is $5\varepsilon_0$ and the frequency is 50 Hz.

The second case, from [56], which gives some grounding impedance measurement results, two types of grids are used for the measurements: grid (a) is 100 m × 100 m 16-mesh grid, grid (b) is a 50 m × 50 m 16-mesh grid. The earth is considered as a half uniform medium. The radius of the grid conductors is 0.5 cm, and they are buried at a depth of 0.5 m in the earth. Here, the conductivity of the copper conductors is $\sigma_{Cu} = 5.8 \times 10^7$ S/m, and the permittivity of the earth model is set at $\varepsilon_1 = 5$. The result can be seen in Tables 1 and 2.

Table 1. Comparison with published measurement result: Uniform earth model ($\sigma = 10^{-2}$ S/m) $f = 80$ Hz.

grid type	Ref. [56]	Our model	
grid	Meas.	Quasi-static	Dynamic state
a	0.52	$(0.55, 1.65 \times 10^{-4})$	$(0.54, -1.25 \times 10^{-2})$
b	0.99	$(1.04, 3.11 \times 10^{-3})$	$(1.03, -1.03 \times 10^{-2})$

Table 2. Comparison with published measurement result: uniform earth model ($\sigma = 10^{-1}$ S/m) $f = 80$ Hz.

grid type	Ref. [56]	Our model	
grid	Meas.	Quasi-static	Dynamic state
a	0.05	$(0.07, 1.35 \times 10^{-4})$	$(0.07, -3.00 \times 10^{-3})$
b	0.10	$(0.12, 2.90 \times 10^{-3})$	$(0.12, -1.04 \times 10^{-3})$

6.1.2. High Frequency Domain Case

The first case shows different frequency grounding impedances between our code and the measurement data from [57]. In this case, vertical conductors with 4 m length have been buried in a homogenous earth model with $\rho_e = 450\,\Omega$m, and the permittivity used in our model is, respectively, set as $\varepsilon_e = 10$,

$\varepsilon_e = 40$ and $\varepsilon_e = 80$. The comparison can be seen in Fig. 2. It can be seen that they are in agreement with each other for high frequencies.

The second case also gives the comparison from low frequency to higher frequency between our code and the simulation results from [58], a horizontal conductor with 1 m length and 5 mm radius was buried at 1 m depth below a homogenous earth model, which possesses $\rho_e = 100\,\Omega$m and $\varepsilon_e = 10$. It is seen in Fig. 3 that they agree with each other from low frequencies to higher frequencies.

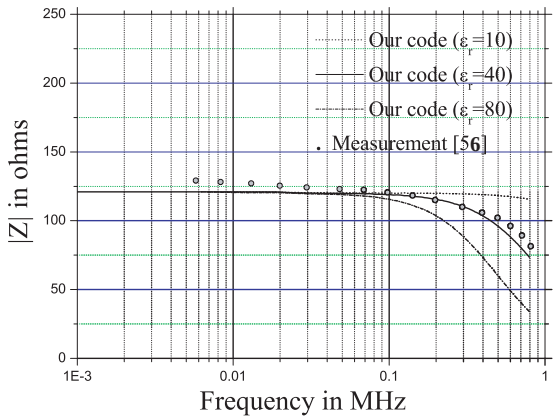

Figure 2. Comparison of grounding impedance dependence on frequency between the measurement data from [57] and our code.

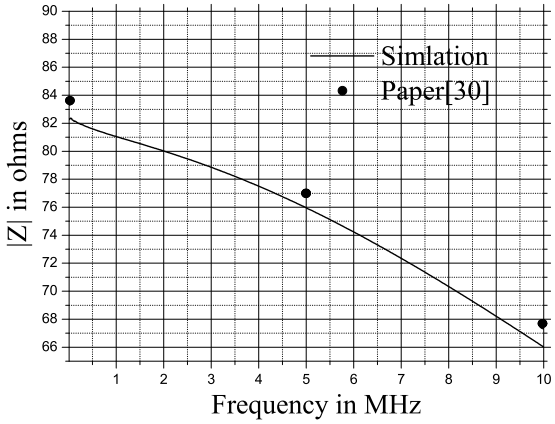

Figure 3. Comparison of grounding impedance dependence on frequency between the numerical results from [58] and our code.

6.1.3. Time Domain Case

The case from [45], a typical grounding grid with a 2×2 mesh grid and with the size of 10×10 m is considered, which was made of round copper conductors with a 50 mm^2 cross section. The grounding grid was buried at 0.5 m depth in two-layer horizontal earth, whose resistivity's ratio for the upper and the lower soil layers is $\rho_1/\rho_2 = 50/20\,\Omega$m/$\Omega$m, the upper layer thickness being $H = 0.6$ m. For our method, a homogenous earth model should be used. From [54], the soil apparent resistivity is found to be 43.81 Ωm, and the soil's permittivity is set as 5. The inject lightning current parameter was set at $T_1 = 3.5\,\mu$s, $T_2 = 73\,\mu$s, and $I_m = 12.1$ A. The feed point is at the middle of one border of the grid. The transient SEP can be seen in Fig. 4, which ultimately agrees with the measured curve in Fig. 7(c) in [45]; meanwhile, the impulse grounding impedance was 1.6 Ω, as given by [45], and it is 1.50 Ω for our model.

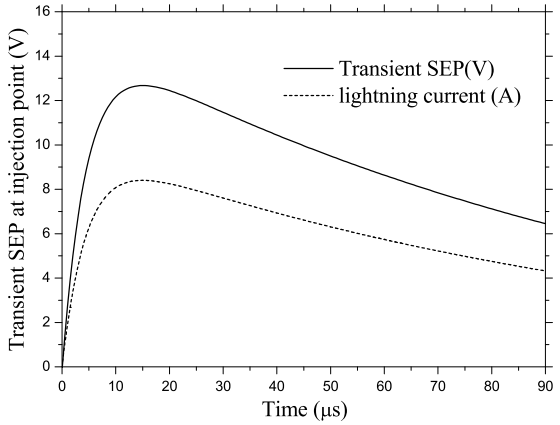

Figure 4. Transient SEP at injection point.

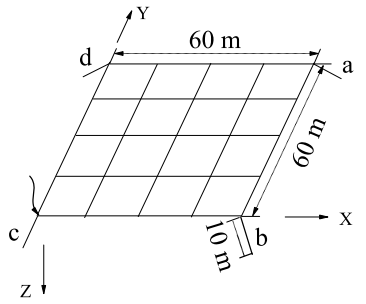

Figure 5. A grounding system.

6.2. Validation of Our Methods

The DSCIM's solution can give less than 1% error, compared to the numerical integration of Sommerfeld, in the near and intermediate zones. In the far zone, however, the complex-image solution gives a large percentage of error for the case of a dipole embedded within lossy ground. In the transient analysis of the grounding system, the maximal frequency is about 1 MHz for the typical lightning current; in this case, the wavelength is approximately 10–30 m for the typical soil parameter. On the other hand, for the far field, the absolute value of the mutual coupling between widely separated segments is negligible. The 1 MHz limit was given by CCITT [59], which is too prudent in our method: actually, the maximum frequency for our method is up to 10 MHz, covering the frequency range usually of interest in power systems.

6.3. Simulation Result Analysis

A grounding system is given in Fig. 5, which is buried below the ground surface at a depth of 0.5 m, four bars with cross angles with the x, y, and z axes of, respectively, $\theta_x = \theta_y = \theta_z = 45°$ for a, $\theta_x = \theta_z = 45°, \theta_y = 135°$ for b, $\theta_x = \theta_y = 135°$, $\theta_z = 45°$ for c and $\theta_x = \theta_z = 45°$, $\theta_y = 135°$ for d. The earth is modeled as a half homogenous conductive medium, whose conductivity and permittivity are $\sigma_1 = 15^{-2}\,\mathrm{S/m}$, $\varepsilon_1 = 20\varepsilon_0$, respectively. The material of the grounding system conductor is Cu with conductivity $\sigma_{Cu} = 5.8 \times 10^7\,\mathrm{S/m}$. The conductor radius is 5 mm. The external excited lightning current is injected from the corner of the grounding system, which is described by a double-exponential function as $I(t) = 1.29 \times (e^{-0.019010t} - e^{-0.292288t})\,\mathrm{kA}$, which means that the parameters of the lightning current are $T_1 = 10\,\mu\mathrm{s}$, $T_2 = 50\,\mu\mathrm{s}$ and $I_m = 1.29\,\mathrm{kA}$.

6.3.1. Discussion of the QSCIM and DSCIM Methods for the Grid

The numerical results can be seen in Fig. 6: we can see that the transient SEP at injection point agree with each other with smaller discrimination from the Fig. 6. Meanwhile, we know that the impulse grounding impedance from QSCIM is $(1.866,\ 2.977 \times 10^{-2})\,\Omega$ and from DYCIM is $(1.777,\ -6.598 \times 10^{-2})\,\Omega$.

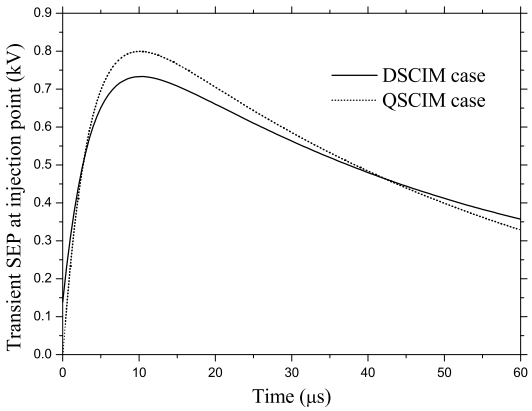

Figure 6. Transient SEP at injection point between dynamic and quasi-static case.

6.3.2. Discuss Electromagnetic Field Distribution above the Grounding System

Three different times (2 μs, 39.5 μs, and 79.5 μs) have been chosen to discuss the electromagnetic field on the ground surface above the grid. Before the discussion, we can observe that the total leakage currents of the grounding system and the harmonic components of external injected currents in the frequency domain in Fig. 4 in Table 3. From the Table, we can see that this model's accuracy is good.

The distribution of the electromagnetic field along the surface with chosen three different times has been given in Figs. 7–12. Among these figures, Figs. 7–9 show the distribution of module of EFI E along the surface, and Figs. 10–12 show the distribution of module of MFI B along the surface.

Table 3. Total currents along grid for different frequencies.

Freq.	Total leakage currents (kA)	Harmonic components (kA)
0.025 MHz	(−4.833, −4.272)	(−4.834, −4.272)
0.5 MHz	$(-0.184, 3.985 \times 10^{-3})$	$(-0.184, 3.988 \times 10^{-3})$
1 MHz	(−5.469, 9.094)	(−5.469, 9.094)

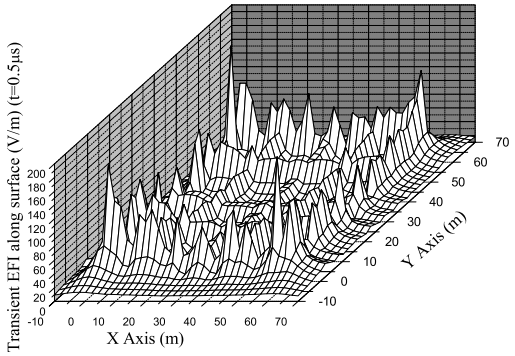

Figure 7. Distribution of module of EFI E_x on the ground surface ($t = 2\,\mu s$).

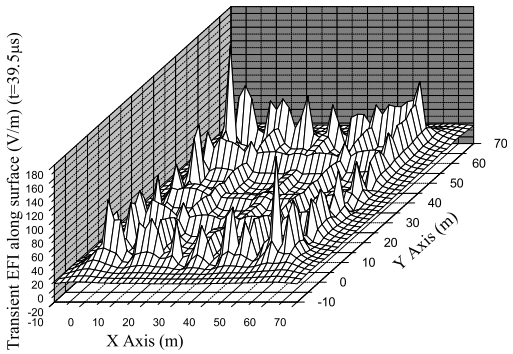

Figure 8. Distribution of module of EFI E_x on the ground surface ($t = 39.5\,\mu s$)

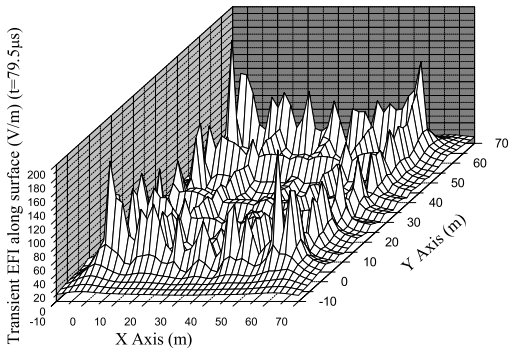

Figure 9. Distribution of module of EFI E_x on the ground surface ($t = 79.5\,\mu s$).

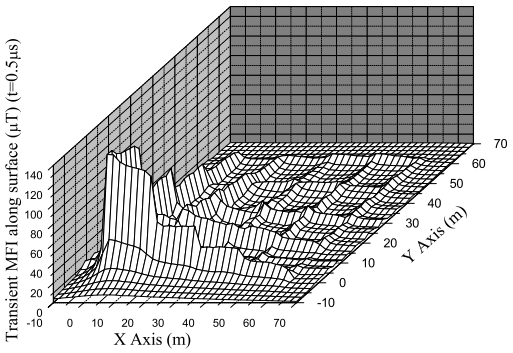

Figure 10. Distribution of module of MFI B_x on the ground surface ($t = 2\,\mu s$).

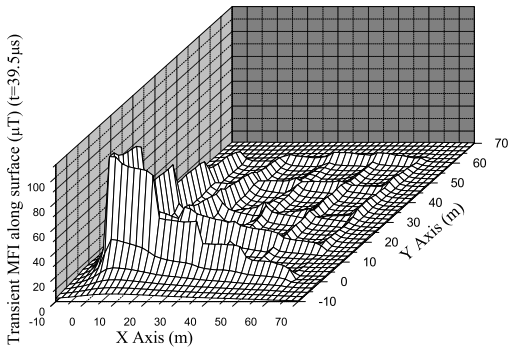

Figure 11. Distribution of module of MFI B_x on the ground surface ($t = 39.5\,\mu s$).

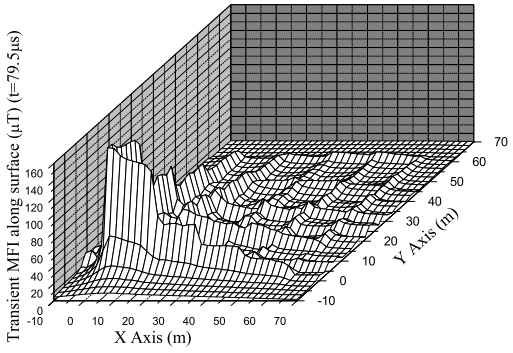

Figure 12. Distribution of module of MFI B_x on the ground surface ($t = 79.5\,\mu s$).

From Figs. 7–9, we can see that the maximum value of the module of EFI E occurs on the four corners instead of the injection point, and the module of EFI E above the injection point is apparently smaller than that above the four corners.

The distribution of the module of MFI B_x is given in Figs. 10–12. We can see that, unlike the EFI case, the maximum value of the module of MFI B occurs at the injection point at the middle of the grid for all times (1 μs, 39.5 μs and 69.5 μs).

7. CONCLUSION

With the FFT, based on the theory of dynamic state electromagnetics, combined with the rapid Galerkin's MoM and the conventional nodal analysis of electrical network model techniques, a new mathematical method for calculating the transient lightning current distribution along a grounding system in the half infinite homogenous earth model for a.c. substations was developed. The DSCIM, a closed form of Green's function for a dipole or monopole buried in the earth, and analytical formulae for the mutual induction and impedance coefficients were introduced into this model to accelerate the calculation. A computer program based on this new mathematical model was developed, which can be applied to investigate a.c. substation transient electromagnetic field distributions and to design a reasonable substation grounding system based on the half infinite homogenous earth model. Last, some numerical results were discussed. In this way, some conclusions have been obtained:

(i) For DSCIM, no pairs of conjugate complex numbers will occur, although they always appear in the QSCIM case.

(ii) The QSCIM assumption provides overestimated results in comparison with the DSCIM case.

(iii) Numerical calculation has been replaced with analytical calculations introduced in our method under the DSCIM approximation for the near field case.

ACKNOWLEDGMENT

This work was funded by the Science and Technology Projects of State Grid Corporation of China under Contract Number: GY172011000JD and the National Natural Science Foundation of China under Grant 51177153.

REFERENCES

1. *IEEE Guide for Safety in AC Substation Grounding*, IEEE Std. 80-2000, 2000.
2. Chowdhuri, P., *Electromagnetic Transients in Power Systems*, Wiley, New York, 1996.
3. Liew, A. C. and M. Darveniza, "Dynamic model of impulse characteristics of concentrated earths," *Proc. Inst. Elect. Eng.*, Vol. 121, 123–135, Feb. 1974.
4. Wang, J., A. C. Liew, and M. Darveniza, "Extension of dynamic model of impulse behavior of concentrated grounds at high currents," *IEEE Transactions on Power Delivery*, Vol. 20, No. 3, 2160–2165, Jul. 2005.
5. Ramamoorty, M., M. M. B. Narayanan, S. Parameswaran, and D. Mukhedkar, "Transient performance of grounding grids," *IEEE Transactions on Power Delivery*, Vol. 4, No. 4, 2053–2059, Oct. 1989.
6. Geri, A., "Behaviour of grounding systems excited by high impulse currents: The model and its validation," *IEEE Transactions on Power Delivery*, Vol. 14, No. 3, 1008–1017, Jul. 1999.
7. Devgan, S. S. and E. R. Whitehead, "Analytical models for distributed grounding systems," *IEEE Transactions on Power Apparatus and System*, Vol. 92, No. 5, 1763–1770, Sep./Oct. 1973.
8. Verma, R. and D. Mukhedkar, "Impulse impedance of buried ground wire," *IEEE Transactions on Power Apparatus and System*, Vol. 99, No. 5, 2003–2007, Sep./Oct. 1980.
9. Mazzetti, C. and G. M. Veca, "Impulse behavior of grounded electrodes," *IEEE Transactions on Power Apparatus and System*, Vol. 102, No. 9, 3148–3156, Sep. 1983.

10. Velazquez, R. and D. Mukhedkar, "Analytical modeling of grounding electrodes," *IEEE Transactions on Power Apparatus and System*, Vol. 103, No. 6, 1314–1322, Jun. 1984.
11. Menter, F. and L. Grcev, "EMTP-based model for grounding system analysis," *IEEE Transactions on Power Delivery*, Vol. 9, No. 4, 1838–1849, Oct. 1994.
12. Liu, Y., M. Zitnik, and R. Thottappillil, "An improved transmission-line model of grounding system," *IEEE Transactions on Electromagnetic Compatibility*, Vol. 43, No. 3, 348–355, Aug. 2001.
13. Liu, Y., N. Theethayi, and R. Thottappillil, "An engineering model for transient analysis of grounding system under lightning strikes: Nonuniform transmission-line approach," *IEEE Transactions on Power Delivery*, Vol. 20, No. 2, 722–730, Apr. 2005.
14. Roubertou, D., J. Fontaine, J. P. Plumey, and A. Zeddam, "Harmonic input impedance of earth connections," *Proc. IEEE Int. Symp. Electromagnetic Compatibility*, 717–720, 1984.
15. Dawalibi, F., "Electromagnetic fields generated by overhead and buried short conductors, Part I — Single conductor," *IEEE Transactions on Power Delivery*, Vol. 1, No. 4, 105–111, Oct. 1986.
16. Dawalibi, F., "Electromagnetic fields generated by overhead and buried short conductors, Part II — Ground networks," *IEEE Transactions on Power Delivery*, Vol. 1, No. 4, 112–119, Oct. 1986.
17. Grcev, L. and Z. Haznadar, "A novel technique of numerical modelling of impulse current distribution in grounding systems," *Proc. Int. Conf. on Lightning Protection*, 165–169, Graz, Austria, 1988.
18. Grcev, L. and F. Dawalibi, "An electromagnetic model for transients in grounding systems," *IEEE Transactions on Power Delivery*, Vol. 5, No. 4, 1773–1781, Oct. 1990.
19. Grcev, L., "Computation of transient voltages near complex grounding systems caused by lightning currents," *Proc. IEEE Int. Symp. Electromagnetic Compatibility*, 393–400, 1992.
20. Grcev, L., "Computer analysis of transient voltages in large grounding systems," *IEEE Transactions on Power Delivery*, Vol. 11, No. 2, 815–823, Apr. 1996.
21. Olsen, R. and M. C. Willis, "A comparison of exact and quasi-static methods for evaluating grounding systems at high frequencies," *IEEE Transactions on Power Delivery*, Vol. 11, No. 3, 1071–1081, Jul. 1996.
22. Grcev, L. and M. Heimbach, "Frequency dependent and transient characteristics of substation grounding system," *IEEE Transactions on Power Delivery*, Vol. 12, No. 1, 172–178, Jan. 1997.
23. Zhang, B., X. Cui, Z. B. Zhao, J. L. He, and L. Li, "Numerical analysis of the influence between large grounding grids and two-end grounding cables by the moment method coupled with circuit equations," *IEEE Transactions on Power Delivery*, Vol. 20, No. 2, 731–737, Apr. 2005.
24. Papalexopoulos, A. D. and A. P. Meliopoulos, "Frequency dependent characteristics of grounding systems," *IEEE Transactions on Power Delivery*, Vol. 2, No. 4, 1073–1081, Oct. 1987.
25. Otero, A. F., J. Cidras, and J. L. Alamo, "Frequency-dependent grounding system calculation by means of a conventional nodal analysis technology," *IEEE Transactions on Power Delivery*, Vol. 14, No. 3, 873–877, Jul. 1999.
26. Visacro, S. and A. Soares, Jr., "HEM: A model for simulation of lightning-related engineering problem," *IEEE Transactions on Power Delivery*, Vol. 20, No. 2, 1206–1209, Apr. 2005.
27. Ala, G., E. Francomano, E. Toscano, and F. Viola, "Finite difference time domain simulation of soil ionization in grounding systems under lightning surge conditions," *Appl. Num. Anal. Comp. Math*, Vol. 1, No. 1, 90–103, 2004.
28. Baba, Y., N. Nagaoka, and A. Ametani, "Modeling of thin wires in a lossy medium for FDTD simulations," *IEEE Transactions on Electromagnetic Compatibility*, Vol. 47, No. 1, 54–61, 2005.
29. Huang, L. and D. Kasten, "Model of ground grid and metallic conductor currents in high voltage a.c. substations for the computation of electromagnetic fields," *Electric Power Systems Research*, Vol. 59, 31–37, 2001.
30. Li, Z. X., W. J. Chen, J. B. Fan, and J. Lu, "A novel mathematical modeling of grounding system buried in multilayer earth," *IEEE Transactions on Power Delivery*, Vol. 21, No. 3, 1267–1272, 2006.
31. Li, Z. X. and W. J. Chen, "Numerical simulation grounding system buried within horizontal multilayer earth in frequency domain," *Communications in Numerical Methods in Engineering*,

Vol. 23, No. 1, 11–27, 2007.

32. Li, Z. X. and J. B. Fan, "Numerical calculation of grounding system in low-frequency domain based on the boundary element method," *International Journal For Numerical Methods in Engineering*, Vol. 73, 685–705, 2008.
33. Ruehli, A. E., "Equivalent circuit models for three-dimensional multiconductor systems," *IEEE Trans. on Microw. Theory and Tech.*, Vol. 22, No. 3, 216–221, Mar. 1974.
34. Ruelhi, A. E. and H. Heeb, "Circuit models for three-dimensional geometries including dielectrics," *IEEE Trans. on Microw. Theory and Tech.*, Vol. 40, No. 7, 1507–1516, Jul. 1992.
35. Aksun, M. I. and R. Mittra, "Derivation of closed form Green's functions for a general microstrip geometry," *IEEE Trans. on Microw. Theory and Tech.*, Vol. 40, No. 11, 2055–2062, Nov. 1992.
36. Dural, G. and M. I. Aksun, "Closed-form Green's functions for general sources and stratified media," *IEEE Trans. on Microw. Theory and Tech.*, Vol. 44, No. 7, 1545–1552, Jul. 1995.
37. Chow, Y. L., J. J. Yang, and G. Y. Delisle, "Discrete image theory for horizontal electrical dipoles in a multilayered medium," *IEE Proceedings — H on Microwave Antenna & Propagation*. Vol. 135, No. 5, 297–303, 1988.
38. Chow, Y. L., J. J. Yang, D. G. Fang, and G. E. Howard, "A closed form spatial Green's function function for the thick microstrip substation," *IEEE Trans. on Microw. Theory and Tech.*, Vol. 39, No. 3, 588–592, Mar. 1991.
39. Hojjat, N., S. Safavi-Naeini, R. Faraji-Dana, and Y. L. Chow, "Fast computation of the nonsymmetrical components of the Green's function function for multilayer media using complex image," *IEE Proceedings — H on Microwave Antenna & Propagation*, Vol. 145, No. 4, 285–288, Aug. 1998.
40. Chow, Y. L., J. J. Yang, and K. D. Srivastava, "Complex images of a ground electrode in layered soil," *Journal of Applied Physics*, Vol. 72, No. 2, 569–574, Jan. 1992.
41. Zhang, L. P., J. S. Yuan, and Z. X. Li, "The complex image method and its application in numerical simulation of substation grounding grids," *Communications in Numerical Methods in Engineering*, Vol. 15, No. 11, 835–839, 1999.
42. Li, Z. X., G. F. Li, and J. B. Fan, "Numerical simulation of substation grounding system in low frequency domain basing on the boundary element method with linear basis function," *Communication in Numerical Method in Engineering*, Published Online: Jun. 12, 2009.
43. Li, Z. X., J. B. Fan, and W. J. Chen, "Numerical simulation of substation grounding grids buried in both horizontal and vertical multilayer earth model," *International Journal for Numerical Methods in Engineering*, Vol. 69, No. 11, 2359–2380, 2007.
44. Andolfato, R., L. Bernardi, and L. Fellin, "Aerial and grounding system analysis by the shifting complex images method," *IEEE Transactions on Power Delivery*, Vol. 15, No. 3, 1001–1009, Jul. 2000.
45. Stojkovic, Z., J. M. Nahman, D. Salamon, and B. Bukorovic, "Sensitivity analysis of experimentally determined grounding grid impulse characteristic," *IEEE Transactions on Power Delivery*, Vol. 13, No. 4, 1136–1143, Oct. 1998.
46. Choma, J., *Electrical Networks — Theory and Analysis*, New York, 1985.
47. Heppe, R. J., "Computation of potential at surface above an energized grid or other electrode, allowing for non-uniform current distribution," *IEEE Transactions on Power Apparatus and Systems*, Vol. 98, No. 6, 1978–1989, 1979.
48. Sarmiento, H. G., D. Mukhedkar, and V. Ramachandran, "An extension to the study of earth-return mutual coupling effects in ground impedance field measurements," *IEEE Transactions on Power Delivery*, Vol. 3, No. 1, 96–101, 1988.
49. Kmayman, N. and M. I. Aksun, "Efficient use of closed-form Green's functions for the analysis of planar geometries with vertical connections," *IEEE Trans. on Microw. Theory and Tech.*, Vol. 45, No. 5, 593–603, May 1997.
50. Chow, Y. L., N. Hojjat, S. Safavi-Naeini, and R. Faraji-Dana, "Spectrum Green's functions for multilayer media in a convenient computaion form," *IEE Proc. — Micow. Antenna and*

Propagation, Vol. 145, No. 1, 85–91, Feb. 1998.

51. Adve, R. S. and T. K. Sarkar, "Extrapolation of time-domain responses from three-dimensional conducting objects utilizing the Matrix Pencil technique," *IEEE Transactions on Antenna and Propagation*, Vol. 45, No. 1, 147–156, 1997.
52. Navarrina, F., I. Colominas, and M. Casteleiro, "Aboundary element numerical approach for grounding grid computation," *Computer Methods in Applied Mechanics and Engineering*, Vol. 174, 73–90, 1999.
53. Li, Z. X., G. F. Li, J. B. Fan, and C. X. Zhang, "Numerical calculation of ac substation grounding systems buried in a horizontal multilayered earth by higher order basis function," *International Journal of Power and Energy Systems*, Vol. 32, No. 1, 21–30, 2012.
54. Mattos, M. A. F., "Grounding grids transient simulation," *IEEE Transactions on Power Delivery*, Vol. 20, No. 2, 1370–1379, Apr. 2005.
55. Ma, J. X. and F. P. Dawalibi, "Modern computation method for design and analysis of power system grounding," *1998 International Conference on Power System Technology Proceedings*, Vol. 1, 122–126, Beijing, China, Aug. 18–21, 1998.
56. Ma, J. X. and F. P. Dawalibi, "Influence of inductive coupling between leads on ground impedance measurements using the fall-of-potential method," *IEEE Transactions on Power Delivery*, Vol. 16, No. 4, 739–743, Oct. 2001.
57. Grcev, L., "High-frequency performance of ground rods in highly resistive soil," *International Conference on Grounding and Earthing*, Belo Horizonte Brazil, Jun. 18–21, 2000.
58. Grcev, L., "Calculation of the transient impedance of grounding systems," Ph.D. Thesis, University of Zagreb, 1986 (in Croatian).
59. CCITT, *Directives Concernant La Protection Des Lignes De Telecomunication Contre Les Actions Nuisibles Del Lignes Electriques*, New Delhi, 1960.